Structure and disorder in ice VII on the approach to hydrogen-bond symmetrization

M. Guthrie, R. Boehler, J. J. Molaison, B. Haberl, A. M. dos Santos, and C. Tulk

Phys. Rev. B **99**, 184112 — Published 23 May 2019

DOI: 10.1103/PhysRevB.99.184112

Structure and disorder in ice VII on the approach to hydrogen-bond symmetrisation.

M. Guthrie[1,2], R. Boehler[3,4], J. Molaison[4], B. Haberl[4], A. M. dos Santos[4] & C. Tulk[4]

[1]*European Spallation Source, Lund, Sweden*

[2]*University of Edinburgh, Edinburgh, UK*

[3]*Carnegie Institution of Washington, Washington, DC, USA*

[4]*Oak Ridge National Laboratory, Oak Ridge, TN, USA.*

ABSTRACT

Using new techniques, we have collected neutron-diffraction of sufficient quality for structural refinement from deuterated ice VII to over 60 GPa. At these pressures, we are approaching the onset of molecular dissociation where the water molecule should be significantly distorted. We fitted our data with both the conventional structural model for ice VII and a recently proposed 'interstitial' model. We found these to be statistically indistinguishable and, therefore, adopted the conventional model in this work. Our refinements yield the first direct experimental determination of the molecular structure in this pressure regime. They show a clear elongation of the covalent bond, the rate of which rapidly increases with pressure, indicating we have entered a new regime on the approach to ice X. In addition, we have directly measured the pressure dependence of the separation of the two equivalent deuteron sites along the hydrogen bonds, which provides an upper bound on the hydrogen-bond centring pressure.

1. INTRODUCTION

Neutron diffraction is the only technique able to spatially locate protons and deuterons within crystalline solids. Such measurements were the first to reveal the familiar bent shape of the water molecule in ice Ih in 1949 [1]. However, until recently, diffraction measurements with neutrons have been limited in pressure to around 20 GPa. Above 2 GPa (depending on temperature), water ice stabilizes in one or the other of the closely related

phases VII or VIII [2]. In this regime, despite having densities that are almost double that of ice Ih, the water molecule is essentially unchanged from that found at ambient pressure [3].

Meanwhile, much of the fundamental interest in high-pressure ice has focused on the idea that, as density increases, the hydrogen bond must gain in strength and ultimately become equivalent in strength and length to the covalent bond. The resulting 'symmetric' phase (now called ice X) where the hydrogen atom is equidistant between both neighbouring oxygen atoms was first proposed by Kamb and Davis to exist "well above 22 GPa" [4]. A wealth of optical[5-11], x-ray diffraction [12,13] and theoretical studies [14,15] in the intervening decades now place the pressure much higher, although there is still a large uncertainty with claims ranging from 60-110 GPa. Perhaps most intriguing is that *prior* to the transition to ice X, there is an expected increase in the importance of quantum effects [15], with comparative measurements of H_2O and D_2O [7,9,10] suggesting that the transition is ~10 GPa higher in pressure in the latter. In particular, an expected onset of quantum tunneling of the protons (or deuterons) allows for multiple intermediate states to exist between the end points of 'normal' molecular ice and non-molecular symmetric ice.

1.1. The covalent bond in high-pressure ice

In the following discussion, we use R_{OH} or R_{OD} to represent the covalent bond length in normal and deuterated ice respectively. Prior to the availability of high-pressure neutron-diffraction techniques, $R_{OH/OD}$ in high-pressure ice phases was inferred from optical measurements of the vibron frequency in ice [16] and trends observed in other strong O-H…O hydrogen-bonded systems [17]. The first direct measurement of R_{OD} under significant pressure came from neutron-diffraction studies of deuterated ice VIII conducted by Nelmes *et al [18]*. Surprisingly, this revealed quite different behaviour from that found from the earlier indirect measurements: the bond length was observed to increase much more slowly with pressure than previously thought. This clearly would have important consequences for modelling of the transition to symmetric ice at higher pressures.

Figure 1 shows the behaviour of R_{OD} in ice VIII as a function of H-bonded O-atom separation R_{OO}, from two datasets published by Nelmes *et al* [3,18]. Both datasets have been merged

and then fitted with a linear regression, which is then extrapolated into the regime of hydrogen-bond centring. Also shown in Figure 1 are *ab initio* calculations by Benoit *et al* at 100 K for the case of both classical and quantum nuclei [15]. Benoit *et al* briefly discuss isotope effects, indicating that the difference between their quantum and classical calculations provide bounds to the expected behaviour of H and D systems respectively. However, it is not clear where precisely D_2O should be expected between the extremes. Benoit *et al* also examined temperature effects, in the classical case, which they demonstrated to be relatively small: an increase of ~0.02 Å in R_{OD} at any given pressure when warming from 100 to 300 K [15].

In both the quantum and classical calculations, a notable increase in curvature is seen at shorter values of R_{OO} prior to hydrogen bond centring (the line where $R_{OD} = R_{OO}/2$). Unfortunately, the measurements of Nelmes *et al* did not reach a high enough pressure to allow a direct comparison between experiment and calculations.

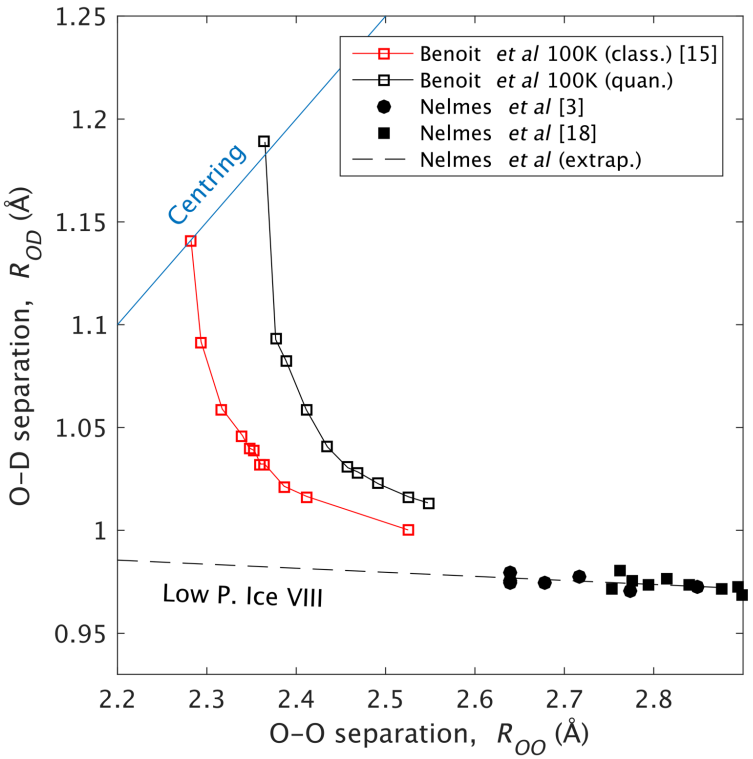

Figure 1 Compares the calculations of Benoit *et al* [15] with the neutron-diffraction measurements of ice VIII by Nelmes *et al* on D_2O [3,18]. A linear fit to the neutron-diffraction measurements extrapolated to short R_{OO} is also shown as a dashed black line. The line labelled "centring" indicates the locus where O-D separation is exactly ½ the corresponding O-O separation.

1.2. Ice VII up to 60 GPa: interstitial ice and the role of disorder

In the present work, we have conducted new neutron powder-diffraction measurements of deuterated ice VII up to ~60 GPa. This is significantly higher than our previous experimental work {Guthrie, 2013 #45}, in which we could only reach 47 GPa {NOTE:Please see discussion of equation-of-state used in Section 2}. At this pressure, the O…O separation is 2.400 Å and so our new measurements bridge the gap between the earlier experimental data and theoretical calculations. Correspondingly, we hope to gain some insight into the behaviour of the water molecule in a pressure regime where it is significantly distorted from its ambient structure. However, some complicating factors must be overcome.

The structure of ice VII

In the crystallographic structure of ice VII (see Section 3.1), the oxygen atoms lie on a bcc lattice with each oxygen surrounded by 8 equidistant neighbours. Each O atom forms hydrogen bonds with four of these neighbours (with two accepted and two donated bonds) to create a tetrahedrally-coordinated network. The remaining four neighbours are themselves bound in a second tetrahedral network that interpenetrates the first. Hydrogen atoms decorate both networks forming water molecules that are arranged so that the Bernal-Fowler ice rules [19] are followed.

Interstitial ice

One issue in interpreting the ice VII diffraction data is the requirement to choose an appropriate structural model. In particular, it was recently proposed by our group [20] that partial molecular dissociation in ice VII may occur at relatively low pressures of ~25 GPa, well below centring. In this ‘interstitial’ model, deuteron density was observed on interstitial locations within the oxygen lattice. The implication was that some ionization of the molecule was occurring, with some free deuterons or deuterium molecules coalescing in the octahedrally-coordinated interstitial volume in the oxygen sub-lattice. However, this model has proven controversial and we have revisited it here.

Disorder

A second fundamental issue is that, unlike ice VIII, ice VII has a highly-disordered structure. Consequently, the average unit cell – as measured in a crystallographic study – differs significantly from the true (instantaneous and local) structure. The disorder in ice VII takes the form of both orientational disorder of the molecules and multi-site disorder of the nuclei. In the former, reorientations allow the molecular dipole to explore the 6 symmetry-allowed positions consistent with the tetrahedral hydrogen-bond network. This results in a crystallographic unit cell where each oxygen is surrounded by four 50% occupied proton/deuteron sites (see Figure 2 [21]). At any instant, the hydrogen/deuterium atoms on any specific molecule will occupy two of these sites. The corresponding sites in the neighbouring H-bonded molecules will be occupied such that the Bernal-Fowler ice rules [19] are observed. In the classical case, thermally-activated concerted reorientations occur rapidly within both hydrogen-bonded networks.

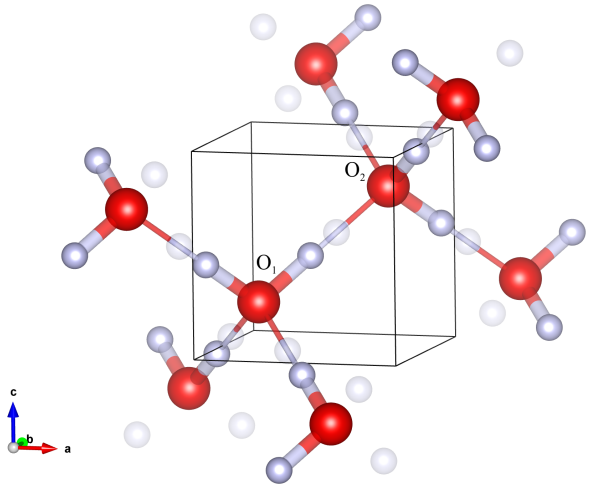

Figure 2 Illustration [21] of a fragment of the local structure of D_2O ice VII (multisite disorder is not shown for clarity) showing one of the two H-bonded networks. O-atoms are shown as larger (red online) and D-atoms as smaller spheres (purple online). The $Pn\bar{3}m$ unit cell is indicated by solid black lines. Covalent bonds are shown as thick bi-color bars joining atoms, while hydrogen bonds are shown as thin bicolour bars, e.g. Atom O_1 donates a hydrogen bond to atom O_2. The two unoccupied D-sites about each O atom are shown as partially transparent spheres.

In the case of multisite disorder, individual nuclei locally explore multiple, symmetry-equivalent sites surrounding their crystallographic average positions [22-24]. This is assumed to arise as a consequence of the mismatch between the perfect tetrahedral coordination of each atom in the average bcc oxygen sub-lattice and the "not-quite-tetrahedral" geometry of the water molecule. Up to the highest pressures where measurements have been conducted (~20 GPa [25]) the water molecule retains its ambient pressure angle of 104.5°, contrasting with the ideal tetrahedral angle of 109.5°. Correspondingly, it is necessary for the oxygen atom to experience a vectorial displacement **δ** off the high-symmetry lattice sites in order to accommodate the molecule within the perfectly cubic metric of the crystallographic lattice (see Figure 3). In ice VIII, a similar effect appears to be at play: without disorder, there is a necessary tetragonal distortion of the unit cell that accommodates the molecule. This tetragonal distortion is related to a spatial offset between the two hydrogen bond networks along the c-axis by an amount ε [18]. Correspondingly, as has been pointed out by Nelmes *et al* [18], there may be an intrinsic relation between magnitude of **δ** in ice VII and the parameter ε in ice VIII.

In principle, it is possible to transform between the local and average positions of atoms if the vectorial displacements from the average sites are known. However, these small displacements have so far proven impossible to measure unambiguously with available crystallographic tools. They have instead been inferred indirectly, for example, Kuhs et al [23] used anharmonic refinements of thermal motion to infer that the O-atoms were displaced along the <100> [26] crystallographic directions by around 0.10 Å. Meanwhile, employing a different approach that used the geometry and thermal motion of the water molecule in ice VIII as a reference, Nelmes et al [25] found a larger magnitude displacement of 0.13 Å along the <111> directions. Although the differences between these two scenarios may seem subtle, in reality, the consequences are dramatic: a <111> displacement breaks the symmetry of the accepted hydrogen bonds creating two distinct H-bond lengths. This would effectively double the configurational entropy of ice VII and add substantial complexity to the VII-X transition. The situation is further complicated as, owing to the slight

difference between the water molecule bond angle and the ideal tetrahedral angle, the D atoms are also expected to be displaced from their average sites [25] by a vector **γ** (also shown in Figure 3). Here, following Nelmes *et al* [25], we assume that γ is directed along the <111>-type directions.

In the following discussion, vectors will be indicated in bold font with their corresponding magnitude having the same symbol in a normal font. For clarity, crystallographic averages will be denoted as barred quantities, for example, the vector $\boldsymbol{R}_{\overline{OD}}$ joins the average O and average D positions, while the vector $\boldsymbol{R}_{OD}$ joins the local positions and has a magnitude, R_{OD} equal the covalent bond length. As above, we will refer to the displacements of the O and D atoms from their average sites by the vectors ***δ*** and ***γ*** respectively.

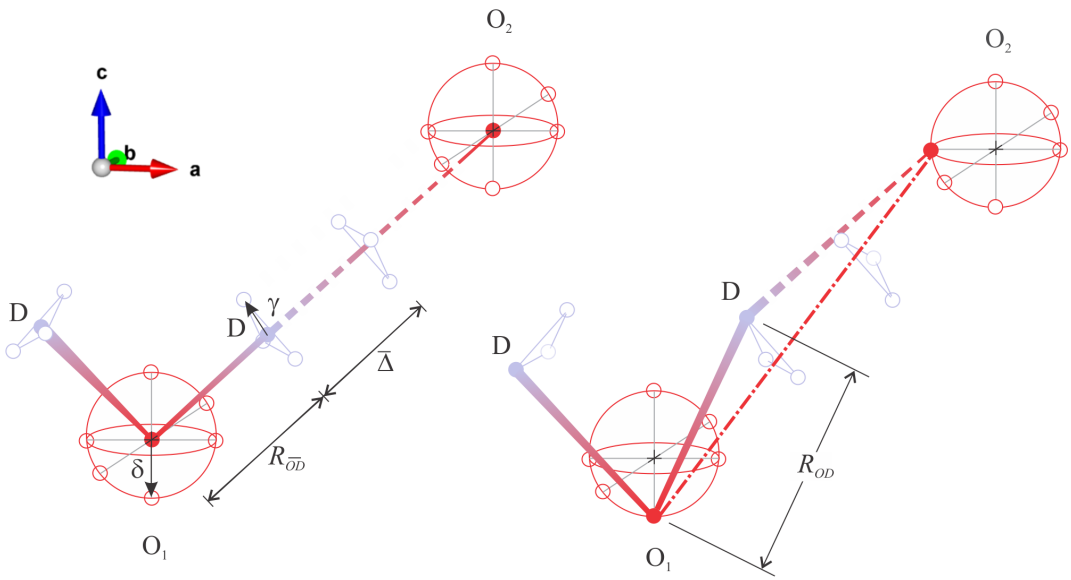

Figure 3 Schematic representation of two H-bonded molecules illustrating some of the possibilities of multisite disorder. For simplicity only one oxygen disorder model, corresponding to a <100>-displacement by an amount δ onto 6-fold equivalent sites, is shown. Open circles indicate symmetry-equivalent possible disordered sites, while full circles indicate occupied sites. O atoms are dark (red online), while D atoms are light (purple online). Meanwhile, the D-atom is shown to be disordered over the 3-fold sites surrounding the <111>-type directions. Solid bi-colour lines indicate covalent bonds, while dashed bi-coloured lines indicate hydrogen bonds. The dot-dashed line (red online) in the right-hand figure indicates the true O…O separation. The left-hand sketch shows the (average) locations that are determined by our crystallographic measurements. The right-hand sketch contrasts this with one possible local arrangement of atoms. The scale is exaggerated to emphasise how the displacement δ leads to a local covalent bond R_{OD} that is significantly longer than the average bond $R_{\overline{OD}}$.

We can relate our crystallographically measured separation $R_{\overline{OD}}$, to the true local covalent bond R_{OD}, by assuming values for ***δ***. Our investigations showed that, as previously noted by

Nelmes *et al* [25], ***γ*** has little effect on R_{OD} as it displaces the D-atom perpendicular to the bond. Meanwhile, the effect of ***δ*** is simply to introduce a constant offset, lowering $R_{\overline{OD}}$ relative to R_{OD}. This effect is found for displacements along both the <100> and <111>-type directions although for a given magnitude of displacement, the offset of $R_{\overline{OD}}$ relative to R_{OD} is larger for the <100> direction. In the analysis that follows in Section 3 we investigate the consequences of different assumptions on the behavior of the *magnitude δ* for both <100> and <111> directions.

2. METHODS

Pure D_2O (Aldrich Chemistry, 99.9% deuterated) was loaded in pre-formed gaskets of 15-5 PH steel that had been heat treated at 482 °C for 2 hours. The initial sample chamber was 157 µm thick with a diameter of ~700 µm, which reduced to ~500 µm after loading. The sample was then sealed in a newly designed diamond-anvil cell [27] at a low pressure of ~ 0.1 GPa and immersed in liquid nitrogen until boiling ceased. At this point, load was increased rapidly using a hydraulic press, which was locked in place using an incorporated screw mechanism. After this point, the cell was allowed to warm to ambient temperature where the sample pressure was measured, by ruby fluorescence spectroscopy [28], to be 11.8 GPa. The resulting thermodynamic route has been found to ensure that a good powder quality of ice VII is generated. This was confirmed by inspecting the intensity of sheets of constant *d*-spacing corresponding to the 110 ice VII reflection measured in all detector pixels. The cell as-loaded, was then inserted in a VX-5 Paris-Edinburgh press which was used to further increase the force on the sample during the subsequent experiment.

A key element of the experimental set-up is that the new cell allowed the use of 6 mm diameter CVD diamonds, 50% larger than those available to us in our previous work [29]. The larger size permitted our 1.5 mm culets to sustain loads in excess of 10.6 tonnes.

Diffraction data were measured on the SNAP diffractometer at the SNS pulsed neutron source, Oak Ridge National Laboratory, USA. The incident beam, collimated to a diameter of ~500 µm using hexagonal boron-nitride pin hole approximately 7 mm upstream of the

samples, was oriented along the load axis of the DAC. Diffracted radiation was then measured in two scintillator-based Anger camera detectors spanning approximately 53 to 97 ° and 83 to 127° in 2θ. Neutrons are counted in the detectors as a function of time-of-flight (TOF), which is related to neutron wavelength (λ) (see e.g. [30]). A calibration measurement of NIST $LaB^{11}{}_6$ was used to determine the conversion needed to render this as a function of *d*-spacing and to calibrate the resolution function of the diffractometer. After converting to *d*-spacing, the individual pixels were summed to give a single average spectrum across both detectors. Prior to summing, pixels with contaminant Bragg reflections from the single-crystal diamonds anvils were masked.

The resulting diffraction pattern is normalized to an equivalent pattern measured from a vanadium rod (ø 650 um) that uses an identical conversion from TOF to *d*-spacing and has been processed with the same diamond-reflection mask. This normalization corrects for factors including the average *d*-dependence of incident neutron flux and detector efficiencies.

An important final correction to the diffraction data, not available in our previous work, was for the effect of the diamond-anvil attenuation on the sample Bragg intensities. As described previously [31], this can be extracted from measurements of the transmission of the incident neutron beam through both upstream and downstream diamonds, which were made by an ORDELA ^{3}He gas monitor. As discussed by Guthrie et al [31], this effect increases markedly with pressure, which strongly enhances internal strain of the anvils with a significant impact on the sample diffraction intensities. As discussed in detail below, this correction was found to be especially important for diffraction measurements of ice VII.

Pressure determination

In our previous work [20], we used the Vinet equation of state reported by Somayazulu *et al* [32]. Here, we have adopted the Birch-Murnaghan equation of state reported by Hemley et al[33], which is based on measurements extending to over 100 GPa. We have compared this with several other equations of state below (see Table 1). Later in this manuscript, we compare our data with measurements conducted at the ISIS Neutron Facility. These

experiments employed a Murnaghan equation-of-state calculated using the *Birch-Murnaghan* parameters reported by Hemley et al [34]. This leads to a significant overestimation of the reported pressures for the ISIS datasets. Correspondingly, to enable comparison, the ISIS datasets shown later have had their pressures adjusted to correspond to the full Birch Murnaghan equation of state by Hemley *et al* and, thus, comparisons with our data occur at equivalent lattice parameters.

3. RESULTS AND DISCUSSION

3.1. Refinements and crystallographic models

The first model we employed in our refinement corresponds to the conventional structure of ice VII[23]. In this model, we include the effect of orientational disorder, but *neglect* the effect of multisite disorder. To do this, we use a "high-symmetry" model that places the O and D atoms on their average sites: (¼,¼,¼) and (x,x,x) respectively of the $Pn\bar{3}m$ space group.

In addition, we also refined a model that allowed for the possibility of interstitial deuterons as per our previous work [20]. The only difference with the conventional model is that a second interstitial D-site is introduced on the (¾,¾,¼) position. The fractional occupancies of both deuteron sites were then allowed to vary, under the constraint that the overall stoichiometry is unchanged. Consequently, this interstitial model has a single additional parameter (the deuterium occupancy) compared to the conventional model.

In initial refinements, both models included an isotropic atomic displacement parameter (ADP) for each atom, which was constrained to be the same for both D atoms in the interstitial model. However, the resulting ADPs were found to be poorly determined. This was attributed to the relatively low signal-to-noise of our data at short *d*-spacings (see Figure 4) and, in subsequent refinements, the ADP's were fixed to values obtained by extrapolation of lower pressure measurements (see supplementary material). Tests showed that the refined deuteron coordinates were unaffected by this constraint within the experimental uncertainties.

The Rietveld fit of the conventional model to our lowest pressure 12.5 GPa data is shown in Figure 4 and illustrates some salient points of the data quality.

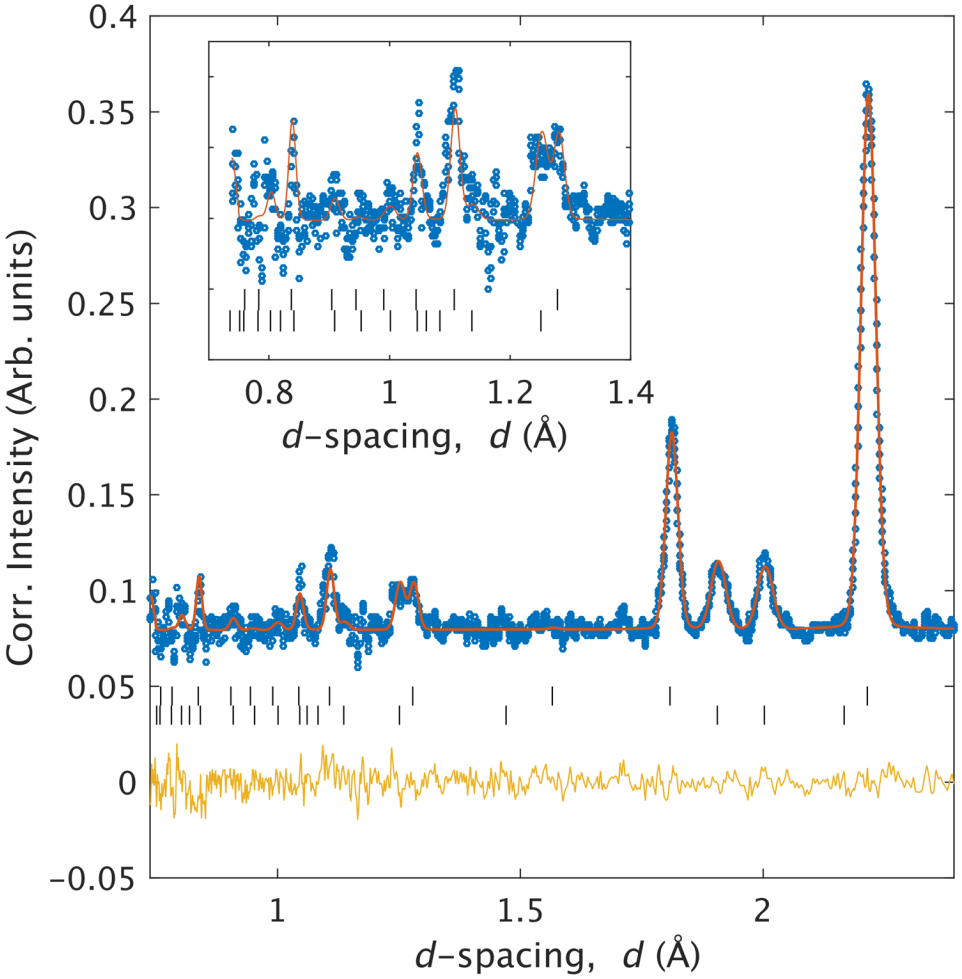

Figure 4 Rietveld fit to diffraction data at 12.5 GPa. Small, open circles (blue online) show normalised and corrected measured diffraction intensities. The solid line running through these (red online) is the Rietveld fit. Upper vertical bars indicate peak positions for the sample, ice VII and lower bar indicate hexagonal Fe from the gasket. The line centred on y=0 (orange online) shows the residual indicating the difference between model and data. Inset shows a close-up of the low-*d*-spacing part of the pattern

Firstly, we note the presence of contaminant scatter from the steel gasket. At all of the pressures measured, this was stable in the ε-iron form. Refinements indicate that the molar ratio of iron from the gasket to ice is initially 24%. This then drops rapidly, reaching a minimum of 2% by 50.6 GPa before increasing again to 17% at the highest pressure (see SM and Figure 5). This is attributed to initial expansion of the inner diameter of the gasket, followed by movement of the gasket hole off centre. Due to the moderate amount of gasket contamination and to best take account of any effect on the sample Bragg intensities, a

separate measurement using synchrotron x-rays was used to characterise the preferred orientation (PO) of the gasket material as a function of pressure (see SM). The observed PO was well described with a single-parameter March-Dollase model [35,36] and was found to be approximately pressure independent (see SM). Subsequently, in the analysis of the neutron data, the same model and same parameters were applied to the gasket phase and kept fixed during the refinements.

A second observation, seen clearly in Figure 4, is that the signal-to-noise ratio at low *d*-spacings is relatively low, although clear peaks are visible down to around 0.8 Å. This is due primarily to the higher background at short *d*-spacings, which correspond to higher energy neutrons in a time-of-flight measurement.

The subsequent evolution of the diffraction pattern with pressure is illustrated in Figure 5.

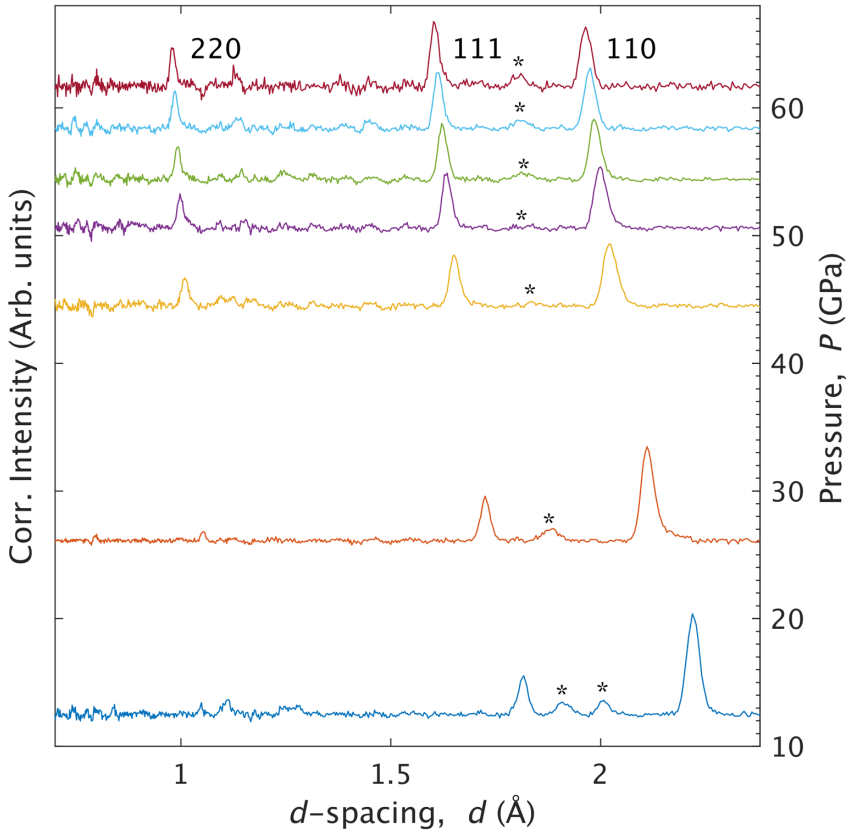

Figure 5 Pressure dependence of diffraction pattern. Data have been scaled by a constant factor and then shifted such that they cross the right hand vertical axis at their measurement pressure. Asterisks indicate the main peak(s) of the (predominantly iron) gasket scattering (note, at the lowest pressure, a mixture of α and ε forms of iron are observed). The 110,111,220 peaks of the ice VII diffraction pattern are labelled by their indices.

These data can be compared with previous measurements made up to 47.0 GPa (on the Hemley *et al* equation of state [33], reported as 43.3 GPa on the Somayazulu *et al* equation of state [32]) used previously by our group [20]. While the relative intensity of the 220 reflection is seen to strongly increase with pressure, as in the previous work, the notable growth of the 111 reflection seen here, was not detected earlier.

A clear explanation for this difference seems to be our applied correction for diamond-anvil attenuation, which was not available in the earlier study. At that time, the effect of the diamond attenuation was measured at ambient pressure and corrected for [37]. However, it was subsequently suggested [38] that there may be a strong enhancement of this attenuation as anvil strain increases under pressure. Follow-up measurements indeed demonstrated that this is the case and a detailed methodology was developed for measuring the effect and applying a correction [31].

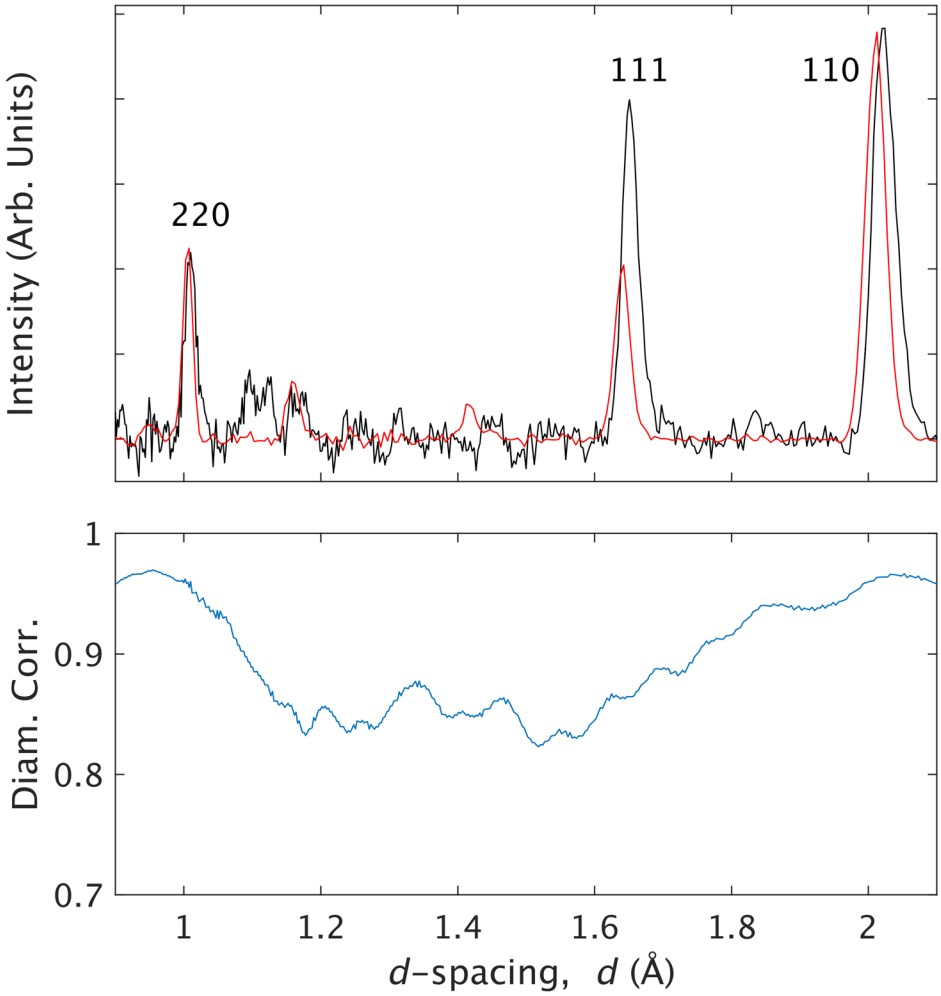

Figure 6 Upper panel shows comparison of current data at 44.5 GPa (black) - corrected for diamond attenuation - with earlier data from Guthrie et al measured at 47.0 GPa (light grey, red online) – uncorrected for diamond attenuation. The indices marking the 110, 111 and 220 reflections, which are the strongest in the pattern. Lower panel shows the correction for diamond attenuation that has been applied to the present data. The 'as measured' data are corrected by dividing by the diamond correction, so it is evident that while the 110 and 220 are little affected, the 111 intensity is significantly increased.

The magnitude of the effect is illustrated clearly in Figure 6, which also highlights the extent of the differences in relative intensities of the 111peak in the previous and current datasets. Indeed, ice VII appears to be a pathological case, where the 110 and 220 reflections both lie outside the largest dip in transmission through the diamond, while the 111 reflection lies well inside, experiencing almost maximum attenuation. We note that the large difference in measured intensity of the 111 reflection in the present (attenuation-corrected) data with the earlier, (uncorrected) data suggests that the diamond attenuation effect was much stronger in the latter. This is perhaps not surprising as, although the culet sizes were the same, the earlier study used 4 mm diameter diamonds (versus the 6 mm anvils in the

present work) and this would result in much larger anvil strain [31]. As the 111 reflection is due only to the presence of the deuteron (the reflection is not observed in x-ray measurements, which are insensitive to proton/deuterons), we might correspondingly expect to see important differences in the behaviour of deuterons in the refined structure.

As shown in Table 1, we see no evidence of the sudden decrease in quality of fit of the conventional model that was previously observed above ~25 GPa. Although the interstitial model does give slightly better fits across much of the pressure range, this can be attributed to the additional parameter lending the model additional flexibility to 'over fit' the data. Correspondingly, there is no longer any empirical or theoretical evidence to justify the interstitial model.

Table 1 Summary of experimental runs used in this work. Four equations of state are given, taken from Hemley et al[33] , Sumayazulu et al [32] and Klotz et al[39]. The last two columns compare the quality of fit for the conventional ("conv.") and interstitial ("int.") models.

Expt. Run	**latt. par. (Å)**	**Pressure (GPa)**				**wRp % (conv.)**	**wRp % (int.)**
		Hemley (B-M)	**Somayazulu (V)**	**Klotz (B-M)**	**Klotz (V)**		
37008	3.1286	12.5	10.0	11.4	11.4	*2.53*	*2.46*
37011	2.9749	26.1	22.0	25.8	25.4	*2.76*	*2.76*
37014	2.8494	44.5	40.6	47.6	45.8	*2.87*	*2.74*
37015	2.8174	50.6	47.2	55.3	52.9	*2.89*	*2.72*
37021	2.7992	54.5	51.5	60.2	57.3	*2.68*	*2.47*
37022	2.7818	58.4	55.8	65.4	61.9	*2.85*	*2.62*
37025	2.7678	61.7	59.6	69.8	65.8	*3.86*	*3.7*

Subsequently, we revisited our Rietveld fits to examine the pressure dependence of the structure of ice VII within the conventional model.

3.2. Determination of the covalent bond in ice VII at high pressure.

As described in Section 1.2 the primary effect of multisite disorder on the covalent bond length R_{OD} comes from $\boldsymbol{\delta}$, which introduces a constant offset of $R_{\overline{OD}}$ relative to this. Here, we explore the consequences of different assumptions on $\boldsymbol{\delta}$. Firstly, if we completely neglect disorder, such that the magnitude of $\boldsymbol{\delta}$ is zero then, in agreement with all previous studies [3,23,24], the covalent bond length is significantly shorter than the actual bond length, taken to be equivalent to that in ice VIII (see discussion in Section 1.2).

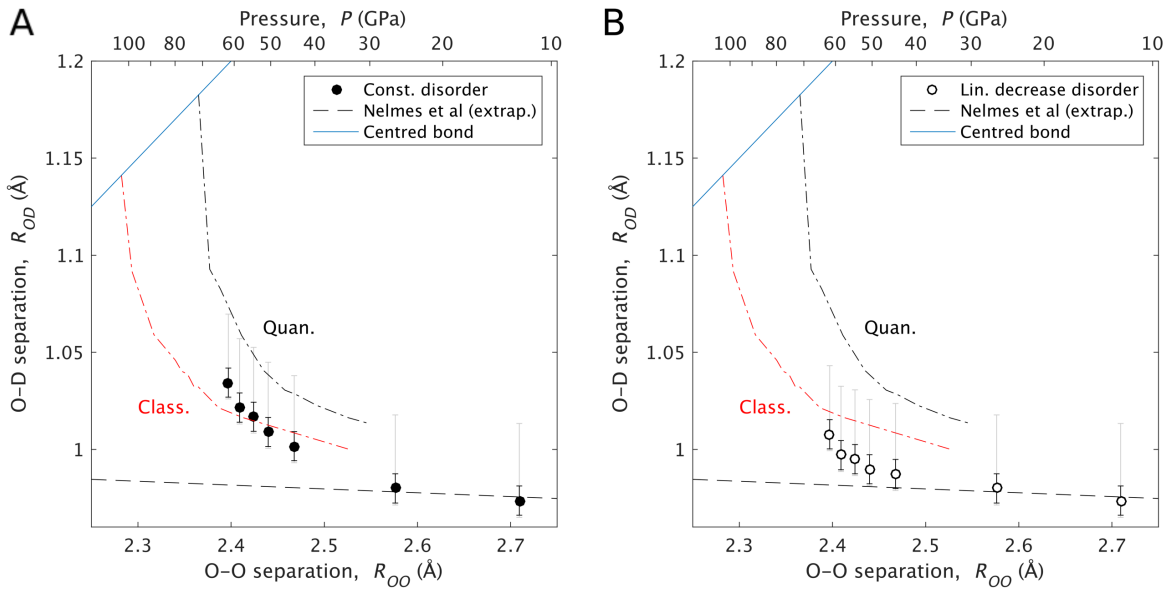

Figure 7 O-D separations determined from our ice VII measurements under the two different assumptions of disorder - that of constant δ (filled circles, Panel A) and that of linearly decreasing δ (open circles, Panel B) – which are compared with the extrapolated ice VIII experimental values from Nelmes et al (Figure 1) (black dashed line). Dark error bars correspond to the uncertainty taken from the Rietveld refinement, light grey error bars represent possible additional shift due to PO (see S.M.). The solid line top left (blue online) shows the locus of centred O-D separations. The pressure corresponding to a given O-O is shown along the top axis and is directly extracted from Helmey *et al*'s equation of state [33]. Also shown are the calculated values from Benoit et al [15] as dot-dashed lines, which are labelled for the quantum and classical case.

By comparing our measurements with those of Nelmes *et al* [18] of ice VIII at overlapping pressures, the shortening to be ~0.04 Å. This offset corresponds to a magnitude δ of 0.11 Å for a <111> displacement and 0.07 Å for a <100> displacement.

The thermal motion measurements of Nelmes *et al* [3,25] demonstrated that δ remains unchanged up to 20 GPa, but we do not know how this changes at higher pressures. However, we can explore the implications of different assumptions on how the multisite disorder changes with pressure on R_{OD}. A limiting assumption would be that the magnitude of the multisite disorder remains unchanged across our pressure range. The corresponding R_{OD} from our measurements is shown in Figure 7A. This shows the clear onset of elongation for O…O separations below ~2.55 Å.

However, it is perhaps unlikely that the multisite disorder would persist unchanged up to centring. To examine this, we considered a simple model where the magnitude δ reduces in a linear fashion below a critical R_{OO} (we arbitrarily chose 2.55 Å to be in the vicinity of the change in slope of the average $R_{\overline{OD}}$), such that, at centring (again chosen arbitrarily to lie between the quantum and classical calculations of Benoit et al at 2.32 Å), δ=0. The results, shown in Figure 7B, also show clear evidence of covalent bond elongation albeit at a lower rate than the constant disorder model.

As discussed in SM, we conducted a detailed investigation of the possibility of PO being present in our sample. We concluded that, although there was no evidence for the presence of PO, we could not completed exclude the possibility that some is present. Correspondingly, we also represent in Figures 7 A&B the effect of PO, should it be present, as gray-colored error bars. If PO is present, the effect is seen to *increase* the value of $R_{\overline{OD}}$

Thus, independent of our assumption of the nature of the multisite disorder, we see the first direct evidence of covalent bond lengthening by a significant amount in ice. This conclusion would be unchanged by the presence of sample PO.

Deuteron site separation

An additional measurement obtained from our refinements is the average location of the two equivalent partially-occupied deuterium sites. As illustrated in Figure 3, these average locations lie along $\boldsymbol{R}_{OO}$. These sites can be conceptualised as reflecting the potential experienced by the deuteron. This potential is symmetric about the mid-point of $\boldsymbol{R}_{OO}$ and, at

low pressure, where molecules are well separated, it has two minima, separated by a distance Δ, with a local maximum between them. At any instant, on any local bond, the H/D atom will be localised in one or the other minimum and covalently bonded to the neighbouring O atom. The energy barrier at the midpoint represents the energy needed for concerted reorientation of both H-bonded molecules such that the Bernal-Fowler ice rules [19] are followed. Benoit et al [15] also studied the behaviour of protons in such a potential and considered quantum effects. In this study, it was found that, when Δ becomes small enough, the onset of quantum tunnelling enables a new route for protons/deuterons to travel from one site to the other.

Our neutron-diffraction measurements are sensitive to the *average* deuteron density and so we are able to measure the average site separation, $\bar{\Delta}$. The resultant value of $\bar{\Delta}$ from our refinement of the conventional model is shown in Figure 8 where it is compared with

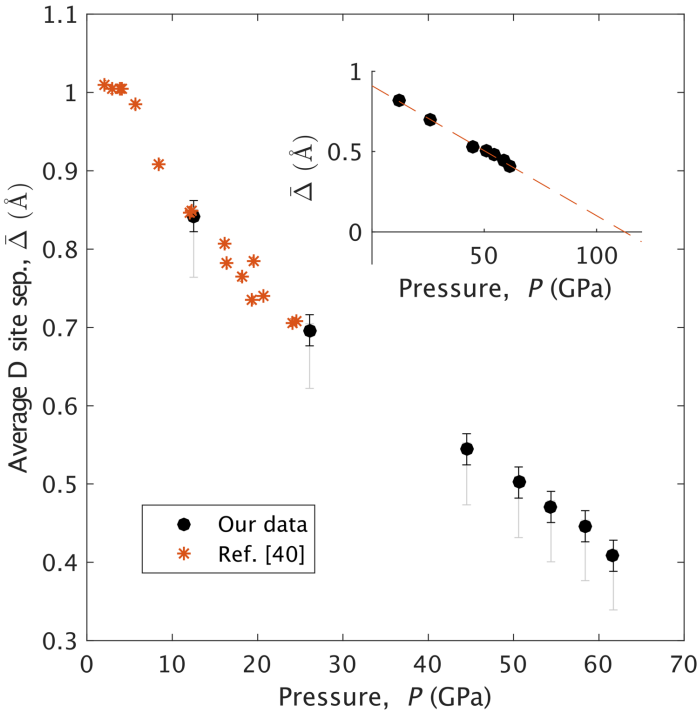

Figure 8 Main figure shows the pressure dependence of $\bar{\Delta}$ up to 60 GPa. Asterisks (red online) show data measured at ISIS in Paris-Edinburgh press from several data sets [40] (note pressures have been adjusted to correspond to the Hemley et al equation-of-state we use, see main text). Solid black circles show the results of our refinement of the conventional ice VII model with black error bars the corresponding uncertainties. Also shown in light grey are is the possible effect of PO (as discussed in the main text and SM). Inset shows the extrapolation of our data points to $\bar{\Delta}$=0.

independent measurements conducted at the ISIS Neutron Facility [40] employing much larger-volume toroidal anvils and Paris-Edinburgh presses.

Overall, the trend shows exceptionally good agreement with the ISIS datasets. Detailed simulations of diffraction patterns (see SM) suggested that the refined value of $\overline{\Delta}$ is primarily dictated by the ratio of intensities of the 111 to 110 reflections. As these are the two strongest peaks in the diffraction pattern, this ratio is well determined in both our datasets and those measured at ISIS. Correspondingly, the good agreement between these two experiments where measurement pressures overlap provides additional confirmation that the new attenuation correction employed is effective. Lastly, we also considered the effect of potential PO in the sample and, if present, this is seen to *decrease* the refined value for $\overline{\Delta}$.

As with the molecular geometry, the multisite disorder (in this case of the deuteron) complicates the interpretation of the crystallographic data, as does the possibility of quantum effects as the deuteron begins to tunnel. Nevertheless, it is interesting to perform a simple linear extrapolation to find where $\bar{\Delta}$ reaches zero. For our $\bar{\Delta}$ values, the extrapolation reaches a value of zero at 112.7 GPa (inset, Figure 8). We also note, however, a suggestion of increased downward curvature in the highest-pressure data point. If this is real, it could point to symmetrisation at significantly lower pressure than the linear extrapolation suggests. In addition, should any PO be present in the sample, this would also tend to reduce the pressure of symmetrisation. We propose that the linear extrapolation provides a plausible upper limit on the symmetrisation pressure.

4. CONCLUSIONS

We have used neutron diffraction to investigate the crystallographic structure of ice VII up to unprecedented pressures exceeding 60 GPa. Under these conditions, the molecule was observed to be significantly modified as a result of a greatly enhanced hydrogen-bond strength. A primary result is that, after improvements in our data-reduction process, we no longer see evidence in the neutron-diffraction data to support the previously proposed ‘interstitial’ model. This important conclusion, brings the neutron-diffraction work in line with previous theoretical and spectroscopic studies and validates the ‘conventional’ model of the ice VII structure in this pressure range.

An intrinsic characteristic of the structure of ice VII and indeed the majority of other molecular ice phases is its disorder. Upon transition to the symmetric phase, there is no longer a distinct molecule and the protons/deuterons are assumed to lie exactly on tetrahedrally-distributed positions. Correspondingly, multisite disorder would therefore be assumed to disappear. If a continuous transition occurred, the molecular angle would gradually increase from 104.5° to the tetrahedral value of 109.5° as the covalent bond lengthened. This scenario would be most closely reflected in our model employing a linear decrease in the magnitude of $\boldsymbol{\delta}$. However, independent of the disorder model we employ, our data show clear evidence that molecular distortion is under way and that we have begun the approach to symmetric ice X.

We have also been able to determine the average site separation of the D atoms which, up to our maximum pressure, is seen to decrease in a linear fashion. A simple extrapolation shows that this will reach zero above 110 GPa, corresponding to fully centred ice. However, as seen in the theoretical calculations shown in Figure 1, significant increase in rate of increase of R_{OD} *versus* O…O is predicted on the approach to symmetrisation. This would imply that ice X is realised at a significantly lower pressure and suggests 110 GPa is an upper limit and the actual transition pressure.

In summary, we have conducted structural measurements of the water molecule under pressures exceeding 60 GPa. These measurements provide insight into the complex role of disorder on molecular distortion and the eventual transition to non-molecular symmetric ice. With ongoing improvements to neutron sources and the development of new high-pressure instrumentation, it looks likely that structural measurements up to and beyond the ice X transition will soon be possible.

5. ACKNOWLEDGEMENTS

The authors would like to thank Dr J.S. Loveday for useful discussions and assistance in retrieving the ISIS datasets. Neutron diffraction was conducted at the SNAP beamline of the Spallation Neutron Source, a DoE Office of Science User Facility operated by Oak Ridge National Laboratory, managed by UT-Batelle LLC, for the U.S. Department of Energy. X-ray

diffraction was performed at HPCAT (Sector 16), Advanced Photon Source (APS), Argonne National Laboratory. HPCAT operations are supported by DOE-NNSA under Award No. DE-NA0001974, with partial instrumentation funding by NSF. The Advanced Photon Source is a U.S. Department of Energy (DOE) Office of Science User Facility operated for the DOE Office of Science by Argonne National Laboratory under Contract No. DE-AC02-06CH11357.

6. REFERENCES

[1] E. O. Wollan, W. L. Davidson, and C. G. Shull, Phys Rev **75**, 1348 (1949).
[2] V. F. Petrenko and R. W. Whitworth, *Physics of Ice* (Oxford University Press, Oxford, 2002).
[3] R. J. Nelmes, J. S. Loveday, W. G. Marshal, J. M. Besson, S. Klotz, and G. Hamel, Rev. High Press. Sci. Tech. **7**, 1138 (1998).
[4] B. Y. B. Kamb and B. L. Davis, Proc. Nat. Acad. Sci. **52**, 1433 (1964).
[5] K. Aoki, H. Yamawaki, M. Sakashita, and H. Fujihisa, Phys. Rev. B **54**, 15673 (1996).
[6] A. F. Goncharov, V. V. Struzhkin, H. K. Mao, and R. J. Hemley, Phys. Rev. Lett. **83**, 1998 (1999).
[7] A. F. Goncharov, V. V. Struzhkin, M. Somayazulu, R. J. Hemley, and H. K. Mao, Science **273**, 218 (1996).
[8] E. Katoh, M. Song, H. Yamawaki, H. Fujihisa, M. Sakashita, and K. Aoki, Phys Rev B **62**, 2976 (2000).
[9] M. Song, H. Yamawaki, H. Fujihisa, M. Sakashita, and K. Aoki, Phys Rev B **60**, 12644 (1999).
[10] V. V. Struzhkin, A. F. Goncharov, R. J. Hemley, and H. K. Mao, Phys. Rev. Lett. **78**, 4446 (1997).
[11] C. S. Zha, R. J. Hemley, S. A. Gramsch, H. K. Mao, and W. A. Bassett, J Chem Phys **126** (2007).
[12] P. Loubeyre, R. LeToullec, E. Wolanin, M. Hanfland, and D. Häusermann, Nature **397**, 503 (1999).
[13] E. Sugimura, T. Iitaka, K. Hirose, K. Kawamura, N. Sata, and Y. Ohishi, Phys. Rev. B **77**, 1 (2008).
[14] M. Benoit, A. Romero, and D. Marx, Phys. Rev. Lett. **89**, 145501 (2002).
[15] M. Benoit, D. Marx, and Parrinello, Nature **392**, 258 (1998).
[16] D. D. Klug and E. Whalley, J Chem Phys **81**, 1220 (1984).
[17] P. Gilli, V. Bertolasi, V. Ferretti, and G. Gilli, J Am Chem Soc **116**, 909 (1994).
[18] R. J. Nelmes, J. S. Loveday, R. M. Wilson, J. M. Besson, P. Pruzan, S. Klotz, G. Hamel, and S. Hull, Phys Rev Lett **71**, 1192 (1993).
[19] J. D. Bernal and R. H. Fowler, J Chem Phys **1**, 515 (1933).
[20] M. Guthrie, R. Boehler, C. A. Tulk, J. J. Molaison, A. M. dos Santos, K. Li, and R. J. Hemley, P Natl Acad Sci USA **110**, 10552 (2013).
[21] K. Momma and F. Izumi, J Appl Crystallogr **41**, 653 (2008).
[22] R. J. Nelmes, J. S. Loveday, W. G. Marshall, G. Hamel, J. M. Besson, and S. Klotz, Phys. Rev. Lett. **81**, 2719 (1998).
[23] W. F. Kuhs, J. L. Finney, C. Vettier, and D. V. Bliss, J. Chem. Phys. **81**, 3612 (1984).

[24] J. D. Jorgensen and T. G. Worlton, J. Chem. Phys. **83**, 329 (1985).
[25] R. J. Nelmes, J. S. Loveday, W. G. Marshall, G. Hamel, J. M. Besson, and S. Klotz, Phys Rev Lett **81**, 2719 (1998).
[26] Here angled brackets indicate the set of symmetry equivalent crystallographic directions
[27] R. Boehler, J. J. Molaison, and B. Haberl, Rev. Sci. Inst. **88**, 083905 (2017).
[28] H. K. Mao, J. Xu, and P. M. Bell, J Geophys Res-Solid **91**, 4673 (1986).
[29] R. Boehler, M. Guthrie, J. J. Molaison, A. M. dos Santos, S. Sinogeikin, S. Machida, N. Pradhan, and C. A. Tulk, High Pressure Res **33**, 546 (2013).
[30] G. L. Squires, *Introduction to the theory of thermal neutron scattering* (Dover Publications, Mineola, N.Y., 1996).
[31] M. Guthrie, C. G. Pruteanu, M.-E. Donnelley, J. Molaison, A. M. dos Santos, J. S. Loveday, R. Boehler, and C. A. Tulk, J App. Cryst. **50**, 76 (2017).
[32] M. Somayazulu, J. Shu, C. S. Zha, A. F. Goncharov, O. Tschauner, H. K. Mao, and R. J. Hemley, J. Chem. Phys. **128**, 064510 (2008).
[33] R. J. Hemley, A. P. Jephcoat, H. K. Mao, C. S. Zha, L. W. Finger, and D. E. Cox, Nature **330**, 737 (1987).
[34] Priv. Comm J.S. Loveday, University of Edinburgh, UK
[35] A. March, Zeitschrift für Kristallographie - Crystalline Materials **81**, 285 (1932).
[36] W. Dollase, J Appl Crystallogr **19**, 267 (1986).
[37] M. Guthrie, R. Boehler, J. J. Molaison, A. M. dos Santos, and C. A. Tulk, Amer. Cryst. Assoc. Trans. Ser. **44**, 149 (2013).
[38] Priv. Comm. J.S. Loveday & R.J. Nelmes
[39] S. Klotz, K. Komatsu, H. Kagi, K. Kunc, A. Sano-Furukawa, S. Machida, and T. Hattori, Phys Rev B **95** (2017).
[40] M. Guthrie, PhD Thesis, University of Edinburgh, 2002.